Journal Pre-proof

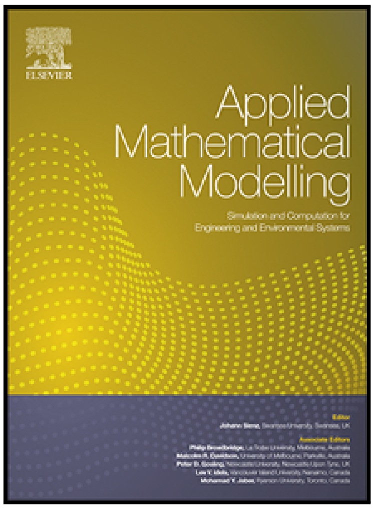

Singular integral equation method for 2D fracture analysis of orthotropic solids containing doubly periodic strip-like cracks on rectangular lattice arrays under longitudinal shear loading

Pengpeng Shi

PII: S0307-904X(19)30556-6
DOI: https://doi.org/10.1016/j.apm.2019.09.026
Reference: APM 13030

To appear in: *Applied Mathematical Modelling*

Received date: 23 August 2018
Revised date: 8 August 2019
Accepted date: 12 September 2019

Please cite this article as: Pengpeng Shi , Singular integral equation method for 2D fracture analysis of orthotropic solids containing doubly periodic strip-like cracks on rectangular lattice arrays under longitudinal shear loading, *Applied Mathematical Modelling* (2019), doi: https://doi.org/10.1016/j.apm.2019.09.026

Highlights

- The orthotropic solids containing doubly periodic cracks is solved.
- The high-precision of the proposed solution is verified.
- Stress intensity factor and crack tearing displacement are studied.
- An analytical formula is proposed for estimating effective shear modulus.

Singular integral equation method for 2D fracture analysis of orthotropic solids containing doubly periodic strip-like cracks on rectangular lattice arrays under longitudinal shear loading

Pengpeng Shi[a,b*]

[a]School of Civil Engineering & Institute of Mechanics and Technology, Xi'an University of Architecture and Technology, Xi'an 710055, Shaanxi, People's Republic of China

[b]State Key Laboratory for Strength and Vibration of Mechanical Structures, Shaanxi Engineering Research Center of NDT and Structural Integrity Evaluation, School of Aerospace, Xi'an Jiaotong University, Xi'an 710049, Shaanxi, People's Republic of China

*Corresponding author: P.P. Shi; E-mail:**shipengpeng@xjtu.edu.cn**

ABSTRACT

The doubly periodic arrays of cracks represent an important mesoscopic model for analysis of the damage and fracture mechanics behaviors of materials. Here, in the framework of a continuously distributed dislocation model and singular integral equation approach, a highly accurate solution is proposed to describe the fracture behavior of orthotropic solids weakened by doubly periodic strip-like cracks on rectangular lattice arrays under a far-field longitudinal shear load. By fully comparing the current numerical results with known analytical and boundary element solutions, the high precision of the proposed solution is verified. Furthermore, the effects of periodic parameters and orthotropic parameter ratio on the stress intensity factor, crack tearing displacement, and effective shear modulus are studied, and an analytically polynomial estimation for the equivalent shear modulus is proposed in a certain range. The interaction distances among the vertical and horizontal periodic cracks are quite different, and their effects vary with the orthotropic parameter ratio. In addition, the dynamic problem is discussed briefly in the case where the material is subjected to harmonic longitudinal shear stress waves. Further work will

continue the in-depth study of the dynamics problem of the doubly periodic arrays of cracks.

KEYWORDS

Integral equation method; orthotropic material; doubly periodic crack; stress intensity factor; crack tearing displacement; effective shear modulus

1. Introduction

In this paper, we discuss the interaction effect of multiple cracks in fracture problems in the context of doubly periodic rectangular lattice arrays of strip-like cracks (DPRC) in an infinite orthotropic solid. The fracture problem of a doubly periodic array of cracks (DPC) has been an open problem for more than 40 years [1]. The DPC requires that cracks are of the same length and arranged in a doubly periodic arrays [1, 2]. The study of such an idealized model can be used to gain insight into complex multiple crack interaction effects in order to analyze the damage and fracture mechanics behaviors of materials [3, 4].

First, we summarize the history of the study of the DPC problem under longitudinal shear load. Much work on the problem of a doubly periodic array of antiplane cracks has focused on fracture studies and equivalent modulus analyses. A number of studies have been devoted to accurately solving the DPC fracture problem. An analytic method was introduced to solve this problem based on a complex function method and doubly periodic function theory [5–6]. Based on the Jacobi elliptic functions, Chang [7] and Kuang [8] obtained general solutions for simply closed forms of the stress intensity factor (SIF) of DPRC subjected to concentrated forces on the surface of each crack. By combining elliptical function theory and a conformal mapping technique, Hao [9] obtained a solution in closed form for a DPC problem with the centers of cracks on the tops of the isosceles triangles. Tong et al. [10] extended Hao's work and derived a closed-form solution for a piezoelectric material with a DPC under a far-field antiplane mechanical load and inplane electrical field. Further studies using similar methods have considered doubly periodic arrays of cracks or rigid-line inclusions in various different materials [11–13].

Many studies have been devoted to the numerical analyses of the DPC fracture problem. Karihaloo [14–16] established a Cauchy kernel singular integral equation with series form for the plane and antiplane problem of DPC, but they did not obtain a numerical solution. By solving the integral equation, Pak and Goloubeva [17] studied the influence of DPRC on the electroelastic properties of piezoelectric materials. Employing oblique coordinates, Malits [18] established a Fredholm integral equation to study the problem of a doubly periodic array of strip-shaped thin rigid inclusions. The work described so far used the integral equation method to solve the DPC problem. Other numerical methods have also been established. Yan and Jiang [19] developed an eigenfunction expansion and variational method for analysis of the DPC problem. Pasternak [20] developed a boundary element method for doubly periodic arrays of cracks and thin in-homogeneities in an infinite magnetoelectroelastic medium. Williams and Parnell [21] proposed a scheme to solve the effective antiplane elastic properties of an orthotropic solid weakened by a DPC. Recently, Shi [22,23] further developed the integral equation method and analyzed the DPC in the periodic layered composite and elastoplastic DPC problems. In particular, the accuracy of this integral equation method has been proven through a comparison of its results with the well-known closed-form solutions [22,23].

The multiple cracks problem has also been used to study elastic wave scattering caused by damage and delamination. For example, by assuming the delamination or damage interface to be a set of multiple cracks, some results related to wave scattering by delamination or damage can be obtained [24]. Many studies have used the spring model to simulate ultrasound interaction with planar damaged interfaces with various structures. Lekesiz et al. [25] obtained explicit analytical expressions for the effective spring stiffnesses of a planar periodic array of collinear cracks between two dissimilar isotropic materials in the two-dimensional (2D) case, and Golub et al. [26] investigated the effective spring boundary conditions for a damaged interface between dissimilar media in the three-dimensional (3D) case. Mykhas'kiv et al. [27] proposed a boundary integral equation method for the investigation of time-harmonic elastic wave propagation through a doubly periodic array of penny-shaped cracks in a 3D infinite elastic solid. Recently, Sumbatyan and Remizov [28] developed a 3D theory for acoustic metamaterials with a triple-periodic array of rectangular-shaped cracks.

The present work constitutes a continuation of the search for a natural and highly accurate solution for fractures in DPRC in infinite orthotropic materials under longitudinal shear loading.

In the framework of a continuously distributed dislocation model, the aim of this study was to reveal the fracture characteristics and predict the effective properties of such cracked materials. To this end, the influences of periodic parameters and orthotropic parameter ratio on the SIF, crack tearing displacement (CTD), and effective shear modulus are studied.

2. Theory/Calculation

2.1 Theoretical model

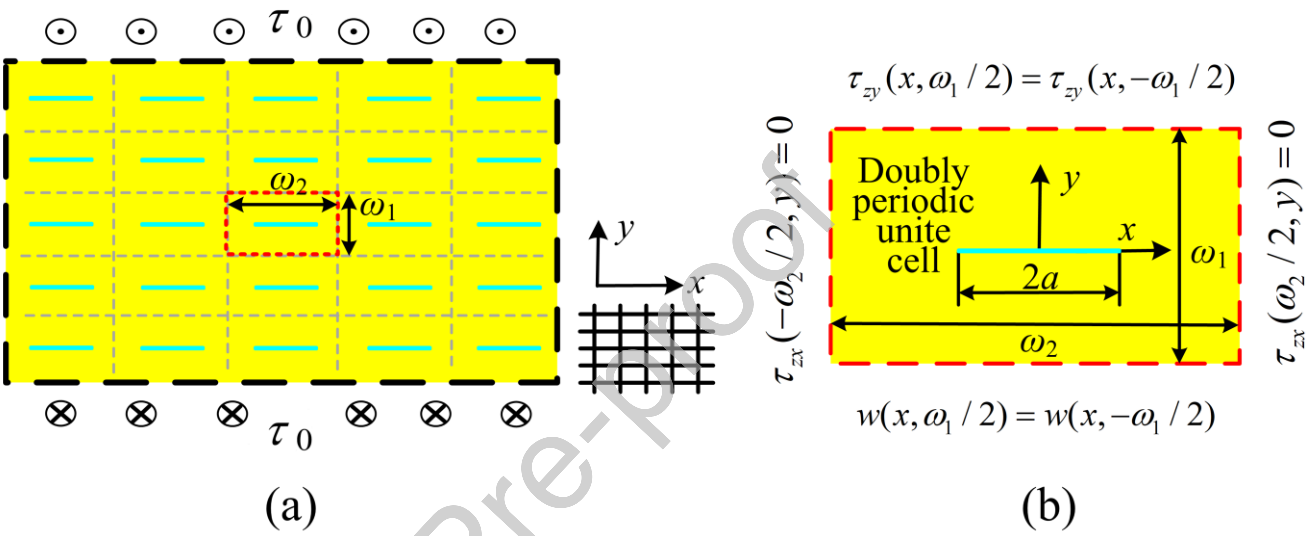

Fig. 1. (a) Doubly periodic crack problems; (b) Rectangular unit cell containing a single crack and its doubly periodic boundary condition for antiplane shear loading.

Figure 1 shows the fracture model, which consisted of DPRC in an infinite orthotropic medium subjected to remote longitudinal antiplane shear loading. The rectangular cells are shown in Fig. 1(b), in which ω_1 and ω_2 are the vertical periodic parameter and the horizontal periodic parameter, respectively; they are also the side lengths of the rectangular unit cells along the x and y directions. The static far-field antiplane shear stress is denoted by τ_0. To solve this static problem, the governing equation and constitutive equation of the orthotropic materials can be written as follows [29]:

$$\tau_{zx}=C_{55}\frac{\partial w}{\partial x},\tau_{zy}=C_{44}\frac{\partial w}{\partial y} \tag{1}$$

$$\frac{\partial \tau_{zx}}{\partial x}+\frac{\partial \tau_{zy}}{\partial y}=0 \quad , \tag{2}$$

where w is the antiplane displacement, τ_{zx} and τ_{zy} denote the antiplane stress, and C_{44} and C_{55} represent the principal shear modulus of the orthotropic material along the y- and x-axes in Fig.

1(a), respectively.

Substituting Eq. (1) into Eq. (2) yields the following governing equation:

$$k^2 \frac{\partial^2 w}{\partial x^2} + \frac{\partial^2 w}{\partial y^2} = 0, \tag{3}$$

where $k = \sqrt{C_{55} / C_{44}}$ is a dimensionless parameter that describes the orthotropic characteristic.

As shown in Fig. 1(b), for remote antiplane shear loadings, the boundary conditions of the rectangle of the unit cell can be described as follows [22,23].

(a) According to the principle of superposition, one can transform the far-field loading $\lim_{y^2 \to \infty} \tau_{zy}(x, y) = \tau_0$ onto the crack surfaces. Then, the linear fracture solution of the DPRC is considered when a pair of the equivalent antiplane shear tractions $\tau(x)=\tau_0$ act on the crack surface. Thus, the boundary conditions at the crack surface in the doubly periodic unit cell can be given as:

$$\tau_{zy}\left(x, 0^+\right) = \tau_{zy}\left(x, 0^-\right), x \in \left(-\omega_2 / 2, \omega_2 / 2\right) \tag{4}$$

$$w\left(x, 0^+\right) = w\left(x, 0^-\right), x \in \left(-\omega_2 / 2, -a\right) \cup \left(a, \omega_2 / 2\right) \tag{5}$$

$$\tau_{zy}\left(x, 0\right) = -\tau_0, x \in \left(-a, a\right). \tag{6}$$

(b) In the DPRC problem, owing to vertical periodicity, the displacements and stress on the upper and lower surfaces of the doubly periodic unit cell are identical [22,23]:

$$\tau_{zy}\left(x, \omega_1 / 2\right) = \tau_{zy}\left(x, -\omega_1 / 2\right), w\left(x, \omega_1 / 2\right) = w\left(x, -\omega_1 / 2\right), \quad x \in \left(-\omega_2 / 2, \omega_2 / 2\right). \tag{7}$$

(c) For the DPRC problem, owing to horizontal periodicity, the periodic boundary conditions imposed on the left and right surfaces of the periodic unit cell are [22,23]:

$$\tau_{zx}\left(-\omega_2 / 2, y\right) = \tau_{zx}\left(\omega_2 / 2, y\right) = 0, \quad y \in \left(-\omega_1 / 2, \omega_1 / 2\right). \tag{8}$$

2.2 Theoretical analysis

In this work, our previously proposed method [22,23] is developed to solve this new problem. By applying the separation variable method, the displacement w and stresses τ_{zx} and τ_{zy} can be given as:

$$w(x, y) = \begin{cases} \sum_{n=0}^{\infty} [A(n) e^{kn\gamma y} + B(n) e^{-kn\gamma y}] \cos(n\gamma x), y > 0 \\ \sum_{n=0}^{\infty} [C(n) e^{kn\gamma y} + D(n) e^{-kn\gamma y}] \cos(n\gamma x), y < 0 \end{cases} \tag{9}$$

$$\tau_{zx}(x,y)=\begin{cases}-\sum_{n=0}^{\infty}C_{55}n\gamma\left[A(n)e^{kn\gamma y}+B(n)e^{-kn\gamma y}\right]\sin(n\gamma x),y>0\\ -\sum_{n=0}^{\infty}C_{55}n\gamma\left[C(n)e^{kn\gamma y}+D(n)e^{-kn\gamma y}\right]\sin(n\gamma x),y<0\end{cases}\tag{10}$$

$$\tau_{zy}(x,y)=\begin{cases}\sum_{n=0}^{\infty}C_{44}kn\gamma\left[A(n)e^{kn\gamma y}-B(n)e^{-kn\gamma y}\right]\cos(n\gamma x),y>0\\ \sum_{n=0}^{\infty}C_{44}kn\gamma\left[C(n)e^{kn\gamma y}-D(n)e^{-kn\gamma y}\right]\cos(n\gamma x),y<0\end{cases},\tag{11}$$

where $\gamma=2\pi/\omega_2$, and the four unknown functions *A*, *B*, *C*, and *D* are to be determined by considering the boundary conditions.

The solution of the above boundary value problem can be found using the CTD or displacement jump on the crack faces:

$$w\left(x,0^{+}\right)-w\left(x,0^{-}\right)=\begin{cases}\int_{x}^{a}a_{l}\left(u\right)du,|x|<a\\ 0,\mathrm{a}<|x|<L\end{cases}.\tag{12}$$

Note that the function $a_l\left(u\right)$ automatically satisfies $\int_{-a}^{a}a_l\left(u\right)du=0$ because of the symmetry of the fracture analysis.

In terms of the Fourier-transformed CTD, the shear stress in the doubly periodic unit cell can be written as:

$$\tau_{zy}(x,y)=\begin{cases}\frac{C_{44}k}{\omega_2}\sum_{n=0}^{\infty}\frac{e^{kn\gamma y}+e^{kn\gamma(\omega_1-y)}}{1-e^{kn\gamma\omega_1}}\int_{-a}^{a}a_l\left(t\right)\sin(n\gamma t)\cos(n\gamma x)dt,y>0\\ \frac{C_{44}k}{\omega_2}\sum_{n=0}^{\infty}\frac{e^{kn\gamma(\omega_1+y)}+e^{-kn\gamma y}}{1-e^{kn\gamma\omega_1}}\int_{-a}^{a}a_l\left(t\right)\sin(n\gamma t)\cos(n\gamma x)dt,y<0\end{cases}.\tag{13}$$

Then, one can transform the crack surface boundary conditions in Eq. (6) into an integral equation:

$$\tau_{zy}\left(x,0\right)=\frac{C_{44}k}{\omega_2}\int_{-a}^{a}\left[\sum_{n=0}^{\infty}\frac{1+e^{kn\gamma\omega_1}}{1-e^{kn\gamma\omega_1}}\sin(n\gamma t)\cos(n\gamma x)\right]a_l\left(t\right)dt=-\tau_0.\tag{14}$$

Next, we recall the identity [22,23]

$$\sum_{n=0}^{\infty}\mathrm{sgn}\left(n\right)\sin\left(\gamma nt\right)\cos\left(\gamma nx\right)=\frac{1}{4}\left[\cot\frac{\gamma\left(t+x\right)}{2}+\cot\frac{\gamma\left(t-x\right)}{2}\right].\tag{15}$$

Now, one can obtain a Hilbert kernel singular integral equation of the first kind:

$$\int_{-1}^{1}\left[\frac{1}{2}\cot\frac{\gamma a(s-r)}{2}-\sum_{n=0}^{\infty}\frac{2\sin(n\gamma as)\cos(n\gamma ar)}{1-e^{kn\gamma\omega_1}}\right]a_l^*(s)ds=\frac{\omega_2\tau_0}{aC_{44}k}, \quad (16)$$

where $s=t/a, r=x/a, a_l^*(s)=a_l(as)=a_l(t)$.

The version of identity Eq. (15) used in previous studies of the periodic crack problem contained some mistakes. These could lead to errors in the derivation of the singular integral equation, which would seriously affect the correctness of the solution to the DPC problem. Here, the correct version of Eq. (15) obtained in our previous work [22,23] is used. Previous researches [22,23] have confirmed that this identity is suitable for solving DPC problems.

2.3 Calculation

According to the theory of singular integral equations, the solution of $a_l^*(s)$ can be expressed as

$$a_l^*(s)=\frac{\omega_2\tau_0}{aC_{44}k}\frac{F(s)}{\sqrt{1-s^2}}, |s|<1, \quad (17)$$

where $F(s)$ is an unknown function to be evaluated numerically, which is continuous and bounded for $|s|<1$ and nonzero at the end points $s=\pm1$. The solution $F(s)$ of the above singular integral equation can be solved numerically using the Lobatto–Chebyshev integration formula [22,23]. Thus, it provides a complete numerical solution of the boundary value problem of DPRC.

3. Results and discussion

In the present work, we are most interested in the following three quantities: SIFs, CTDs, and effective shear modulus of an infinite orthotropic solid with DPRC. In the numerical computations, the material constants of the orthotropic materials are taken to be $C_{44}=E/2/(1+v)$, E=512 GPa, and v=0.3. Given the orthotropic parameter k, the shear modulus C_{55} can be determined by $k=\sqrt{C_{55}/C_{44}}$.

3.1 Stress intensity factors

The most important parameters for crack-tip characterization in linear elastic fracture mechanics are the SIFs. Owing to the symmetry of the problem, only the SIF of the right crack tip is studied here. It is defined by

$$K_{\mathrm{III}} = \lim_{x\to a^+} \tau_{yz}(x,0)\sqrt{2\pi(x-a)} \ , \tag{18}$$

and the stress $\tau_{yz}(x,0)$ at the x-axis is

$$\tau_{yz}(x,0) = -\frac{aC_{44}k}{\omega_2}\int_{-1}^{1}\left[\frac{1}{2}\cot\frac{\gamma a(s-r)}{2} - \sum_{n=0}^{\infty}\frac{2\sin(n\gamma as)\cos(n\gamma ar)}{1-e^{kn\gamma\omega_1}}\right]a_l^*(s)ds \ . \tag{19}$$

This treatment is similar to the approach used by Erdogan and Gupta [30]. The first term in Eq. (19) has a Cauchy-type singularity at $s = r$. To separate this, we observe that around $s = r$,

$$\cot\frac{\gamma a(s-r)}{2} = \frac{2}{\gamma a(s-r)} + o\left(\frac{1}{s-r}\right). \tag{20}$$

Thus, the expression $\tau_{yz}(x,0)$ can be simplified as

$$\begin{aligned}\tau_{yz}(x,0) &= -\frac{aC_{44}k}{\omega_2}\int_{-1}^{1}\frac{1}{\gamma a(s-r)}a_l^*(s)ds \\ &+ \frac{aC_{44}k}{\omega_2}\int_{-1}^{1}\left[\sum_{n=0}^{\infty}\frac{2\sin(n\gamma as)\cos(n\gamma ar)}{1-e^{kn\gamma\omega_1}} - o\left(\frac{1}{s-r}\right)\right]a_l^*(s)ds\end{aligned} \ . \tag{21}$$

For analysis of SIF at the crack tip, only the singular part of the stress needs to be considered. Substituting Eq. (21) into Eq. (18) yields the following expression for the SIF:

$$\begin{aligned}K_{\mathrm{III}}^b &= \lim_{x\to a^+}\tau_{yz}(x,0)\sqrt{2\pi(x-a)} = \lim_{x\to a^+} -\frac{aC_{44}k}{\omega_2}\sqrt{2\pi(x-a)}\int_{-1}^{1}\frac{1}{\gamma a(s-r)}a_l^*(s)ds \\ &= \lim_{x\to a^+, r\to 1^+} -\tau_0\frac{\sqrt{2\pi(x-a)}}{\gamma a}\left(\int_{-1}^{1}\frac{1}{s-r}\frac{F(r)}{\sqrt{1-s^2}}ds + \int_{-1}^{1}\frac{1}{s-r}\frac{F(s)-F(r)}{\sqrt{1-s^2}}ds\right) \\ &= \lim_{x\to a^+}\tau_0\frac{\pi F(1)}{\gamma}\frac{\sqrt{2\pi(x-a)}}{\sqrt{x^2-a^2}} = \frac{\pi F(1)}{a\gamma}\tau_0\sqrt{a\pi}\end{aligned} \ . \tag{22}$$

In the derivation of Eq. (22), the following identity is employed

$$\frac{1}{\pi}\int_{-1}^{1}\frac{1}{(s-r)\sqrt{1-s^2}}ds = -\frac{1}{\sqrt{r^2-1}}, r > 1 \ . \tag{23}$$

Dividing by $\tau_0\sqrt{a\pi}$, the normalized SIF is defined as

$$K_0 = \pi F(1)/a\gamma \ . \tag{24}$$

To verify the correctness of this numerical method, we compared the numerical results for SIF with those of the previous analytical solutions [10,11] and of a numerical solution obtained using the boundary element method [20].

Table 1 presents SIF values for infinite isotropic and orthotropic solids with a DPRC. As shown in the table, as the number of nodes increased, the calculation error of the present results decreased. In particular, when the number of nodes was equal to 20, the absolute error of the results was less than one in ten-thousand, whereas the maximum absolute error of the boundary element method (BEM) is 0.114 [20]. In addition, the numerical method presented in this paper showed very high efficiency for the elongated rectangular doubly periodic case and for orthotropic solids. The comparison of numerical solutions for different node numbers proves that the proposed method has good convergence and high precision.

Table 1. A comparison of dimensionless SIF values obtained using BEM results, analytical solutions, and the proposed numerical solutions

$2a/\omega_2$	0.1	0.2	0.3	0.4	0.5	0.6	0.7	0.8	0.9
$C_{55}/C_{44}=1$, $\omega_1=\omega_2$									
Present solutions, node number = 5	1.00396	1.01632	1.03855	1.073511	1.12627	1.20642	1.33438	1.56417	2.11899
Present solutions, node number = 10	1.00396	1.01632	1.03855	1.073511	1.12627	1.20642	1.33437	1.56396	2.11294
Present solutions, node number = 20	1.00396	1.01632	1.03855	1.073511	1.12627	1.20642	1.33437	1.56396	2.11293
Analytical solutions [10]	1.0040	1.0163	1.0386	1.0735	1.1263	1.2064	1.3344	1.5640	2.1129
BEM with element number= 21[20]	1.0043	1.0167	1.0389	1.0735	1.1266	1.2069	1.3351	1.5660	2.1251
$C_{55}/C_{44}=10$, $\omega_1=\omega_2$									
Present solutions, node number = 5	1.00414	1.01698	1.03983	1.07532	1.12837	1.20846	1.33601	1.56518	2.11937
Present solutions, node number = 10	1.00414	1.01698	1.03983	1.07532	1.12837	1.20846	1.33600	1.56497	2.11332
Present solutions, node number = 20	1.00414	1.01698	1.03983	1.07532	1.12837	1.20846	1.33600	1.56497	2.11331
Analytical solutions [11]	1.0041	1.0170	1.0398	1.0753	1.1284	1.2085	1.3360	1.5650	2.1133
BEM with element number= 21[20]	1.0045	1.0173	1.0402	1.0757	1.1287	1.2089	1.3368	1.5671	2.1255
$C_{55}/C_{44}=0.1$, $\omega_1=\omega_2$									
Present solutions, node number = 5	0.98536	0.95653	0.93852	0.94619	0.98742	1.07189	1.22023	1.48592	2.08498
Present solutions, node number = 10	0.98536	0.95653	0.93852	0.94619	0.98743	1.07194	1.22040	1.48630	2.08099
Present solutions, node number = 20	0.98536	0.95653	0.93852	0.94619	0.98743	1.07194	1.22040	1.48630	2.08099
Analytical solutions [11]	0.9854	0.9565	0.9385	0.9462	0.9875	1.0720	1.2204	1.4863	2.0810
BEM with element number= 21[20]	0.9857	0.9570	0.9391	0.9469	0.9884	1.0731	1.2220	1.4889	2.0922
$C_{55}/C_{44}=1$, $\omega_1=0.05\omega_2$									
Present solutions, node number = 5	0.61072	0.48622	0.45449	0.45639	0.48142	0.53466	0.63705	0.85411	1.49591
Present solutions, node number = 10	0.61077	0.48530	0.45112	0.45341	0.48311	0.54551	0.66214	0.89871	1.53990
Present solutions, node number = 20	0.61077	0.48529	0.45112	0.45348	0.48330	0.54572	0.66211	0.89826	1.54067
Analytical solutions [10]	0.6108	0.4853	0.4511	0.4535	0.4833	0.5457	0.6621	0.8983	1.5407
BEM with element number= 21[20]	0.6117	0.4870	0.4544	0.4594	0.4935	0.5627	0.6906	0.9503	1.6551
Maximum error									
Present solutions, node number = 20	<0.0001	<0.0001	<0.0001	<0.0001	<0.0001	<0.0001	<0.0001	<0.0001	<0.0001
BEM with element number= 21[20]	0.0009	0.0017	0.0033	0.0059	0.0102	0.0170	0.0285	0.0520	0.11403

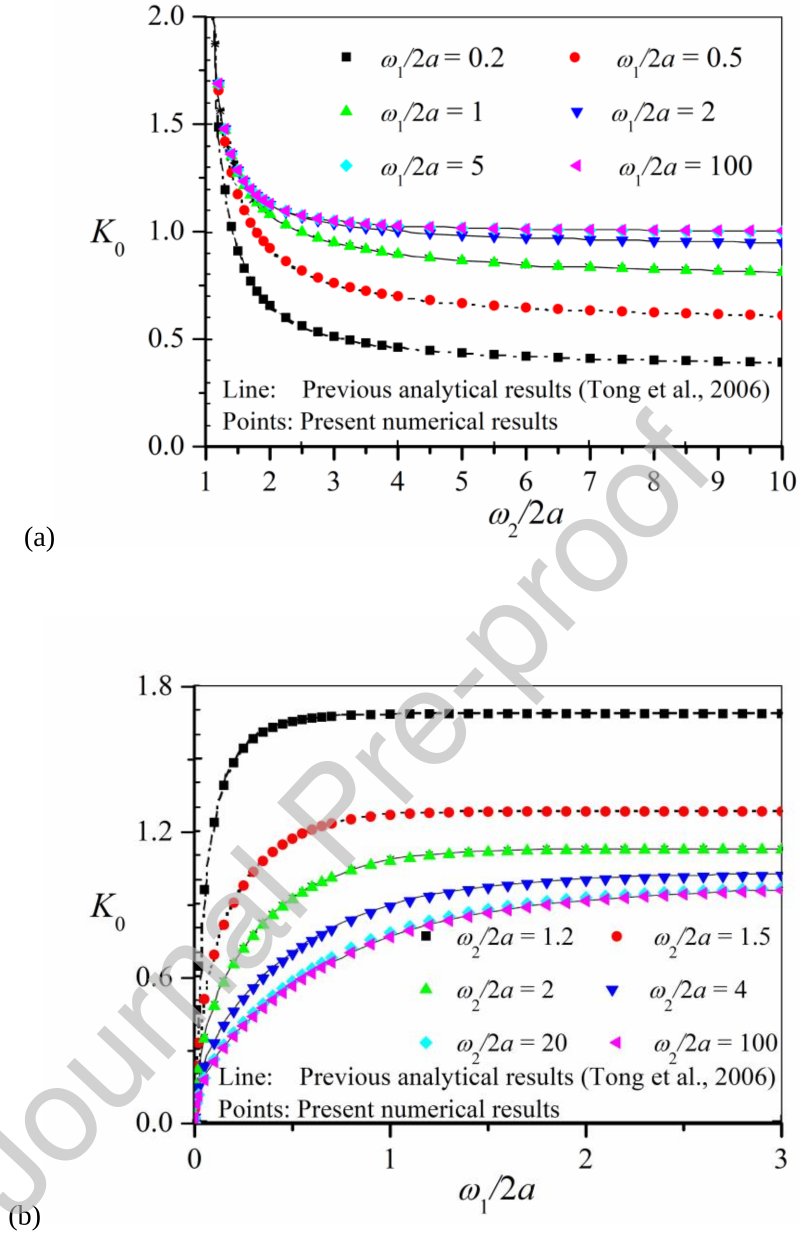

Fig. 2. Variation of the dimensionless SIF with doubly periodic parameters. (a, b) Comparison of SIF with a known solution for isotropic materials.

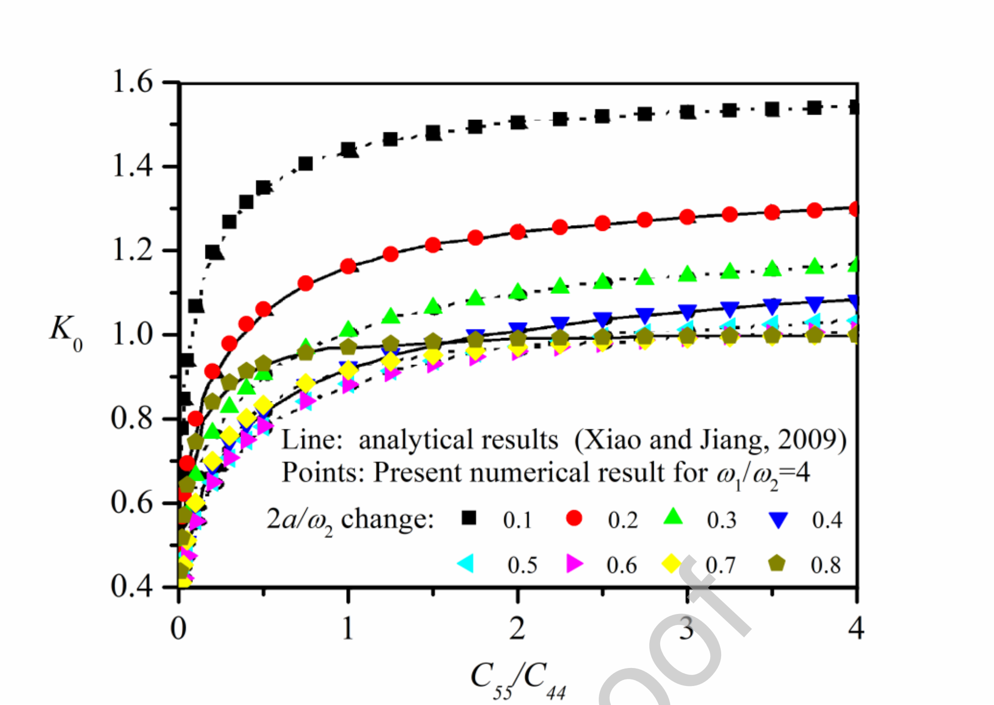

(a)

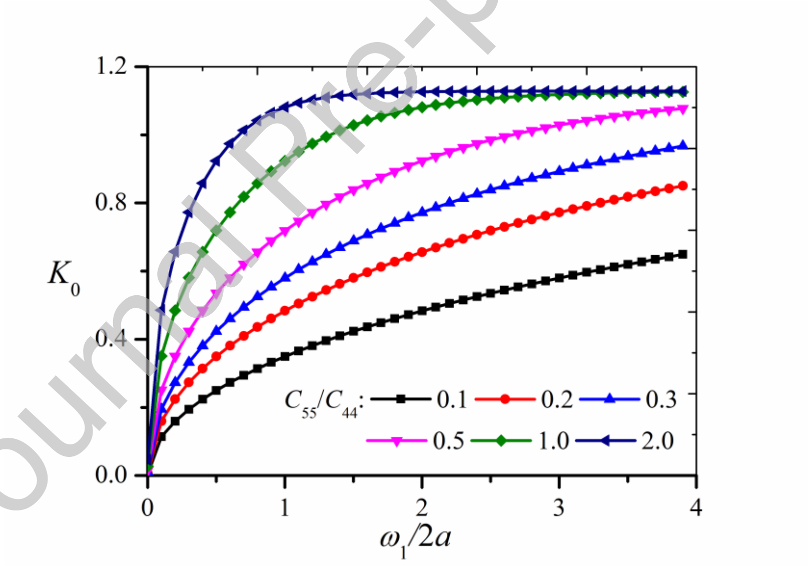

(b)

Fig. 3. Variation of the dimensionless SIF with doubly periodic parameters and orthotropic characteristic. (a) Comparison of SIF with a known solution for orthotropic material; (b) variations in SIF with the vertical periodic parameter and orthotropic characteristic.

Using the complex variables method and elliptical function theory, some closed-form solutions to problems of DCP have been obtained [10,11]. Owing to the specificity of the problem, a previous study [10] of piezoelectric materials resulted in a closed-form solution that was identical to the solution for the DPC problem in isotropic materials. For isotropic and orthotropic materials, respectively, Figs. 2 and 3 compare the results of the present work using the singular integral equation method with results obtained in previous studies [10,11]. The curves obtained by the different methods were exactly the same, and our numerical results were consistent with those of previous studies. This further confirms the correctness of the singular integral equation method presented here. Furthermore, the SIF decreased as the horizontal period parameter ω_2 increased, and increased as the vertical period parameter ω_1 increased. These observations can be explained by the magnification effect of collinear cracks and the shielding effect of horizontal cracks. In addition, for orthotropic materials, the SIF of DPRC strongly depends on the orthotropic parameter; as shown in Fig. 3, the SIF increased as the orthotropic parameter increased.

3.2 Stress field

By using the numerical solution of $F(s)$, the following final expressions for the strain and stress fields of the DPRC problem were obtained:

$$w(x,y)=\begin{cases}\dfrac{\tau_0}{C_{44}}\dfrac{\pi}{m}\displaystyle\sum_{j=0}^{m}\left[\left(\sum_{n=0}^{\infty}\frac{1}{n\gamma k}\frac{e^{kn\gamma(y-\omega_1)}-e^{-kn\gamma y}}{e^{-kn\gamma\omega_1}-1}\sin(n\gamma a s_j)\cos(n\gamma x)\right)\delta_j F(s_j)\right], y>0\\[2ex] \dfrac{\tau_0}{C_{44}}\dfrac{\pi}{m}\displaystyle\sum_{j=0}^{m}\left[\left(\sum_{n=0}^{\infty}\frac{1}{n\gamma k}\frac{e^{kn\gamma y}-e^{-kn\gamma(y+\omega_1)}}{e^{-kn\gamma\omega_1}-1}\sin(n\gamma a s_j)\cos(n\gamma x)\right)\delta_j F(s_j)\right], y<0\end{cases} \tag{25}$$

$$\tau_{zx}(x,y)=C_{55}\frac{\partial w}{\partial x}=\begin{cases}-k^2\tau_0\dfrac{\pi}{m}\displaystyle\sum_{j=0}^{m}\left[\left(\sum_{n=0}^{\infty}\frac{e^{kn\gamma(y-w_1)}-e^{-kn\gamma y}}{e^{-kn\gamma\omega_1}-1}\sin(n\gamma a s_j)\sin(n\gamma x)\right)\delta_j F(s_j)\right], y>0\\[2ex] -k^2\tau_0\dfrac{\pi}{m}\displaystyle\sum_{j=0}^{m}\left[\left(\sum_{n=0}^{\infty}\frac{e^{kn\gamma y}-e^{-kn\gamma(y+w_1)}}{e^{-kn\gamma\omega_1}-1}\sin(n\gamma a s_j)\sin(n\gamma x)\right)\delta_j F(s_j)\right], y<0\end{cases} \tag{26}$$

$$\tau_{zy}(x,y)=\tau_0+C_{44}\frac{\partial w}{\partial y}=\begin{cases}\tau_0+\tau_0\dfrac{\pi}{m}\displaystyle\sum_{j=0}^{m}\left[\left(\sum_{n=0}^{\infty}\frac{e^{kn\gamma(y-\omega_1)}+e^{-kn\gamma y}}{e^{-kn\gamma\omega_1}-1}\sin(n\gamma a s_j)\cos(n\gamma x)\right)\delta_j F(s_j)\right], y>0\\[2ex] \tau_0+\tau_0\dfrac{\pi}{m}\displaystyle\sum_{j=0}^{m}\left[\left(\sum_{n=0}^{\infty}\frac{e^{kn\gamma y}+e^{-kn\gamma(y+\omega_1)}}{e^{-kn\gamma\omega_1}-1}\sin(n\gamma a s_j)\cos(n\gamma x)\right)\delta_j F(s_j)\right], y<0\end{cases}, \tag{27}$$

in which m denotes the numerical quadrature node number, $\delta_0=\delta_m=1/2, \delta_1=\cdots=\delta_{m-1}=1$ is the weight coefficient for the Lobatto–Chebyshev collocation method, and s_j are the Chebyshev collocation points,

$$s_j=\cos\frac{j}{m}\pi,\quad j=0,1,2,\cdots\cdots m. \tag{28}$$

A comparison of the numerical solutions with finite element results for the dimensionless stress τ_{zy}/τ_0 is provided in Table 2 for the case where $\omega_1=\omega_2=4a$. The numerical solution was in excellent agreement with the previous analytical solution for various values of C_{55}/C_{44}. This comparison shows that the numerical method presented in this paper is not only suitable for the analysis of SIF but can also be used to calculate the stress value of each point, with a very high precision. Thus, the calculation results presented here provide a baseline reference that can be used to verify the accuracy of other numerical and approximate methods.

Table 2. Comparison of dimensionless stress between the proposed numerical solution and the previous finite element method (FEM) results and the analytical solution for different C_{55}/C_{44}

C_{55}/C_{44}		*Computational points*				
	Solution method	$(0.5\omega_2,0)$	$(0.5\omega_2,0.25\omega_2)$	$(0.5\omega_2,0.5\omega_2)$	$(0.25\omega_2,0.5\omega_2)$	$(0,0.5\omega_2)$
0.1	FEM results [11]	1.5758	1.5671	1.5549	1.1165	0.2565
	Analytical solutions [11]	1.57786	1.56699	1.55634	1.11571	0.25969
	Present numerical solutions	1.577847	1.566987	1.556341	1.115714	0.259692
1.0	FEM results [11]	1.4175	1.1896	1.0829	1.0006	0.9111
	Analytical solutions [11]	1.41685	1.19142	1.08441	1.00186	0.91188
	Present numerical solutions	1.416838	1.191422	1.084408	1.001863	0.911875
10.0	FEM results [11]	1.4317	1.0054	0.9992	0.9991	0.9990
	Analytical solutions [11]	1.41421	1.00694	1.00010	1.00000	0.99990
	Present numerical solutions	1.414120	1.006937	1.000096	1.0000000	0.999903

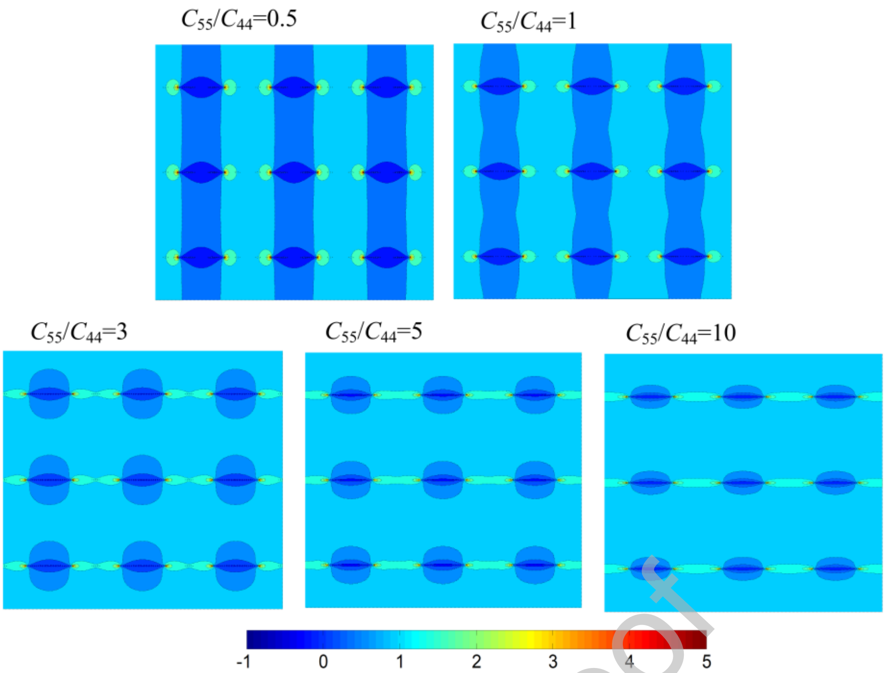

Fig. 4. Contour plot of dimensionless stresses τ_{zy}/τ_0 with different orthotropic parameters.

Figure 4 shows a contour plot of the amplitude of the dimensionless stress τ_{zy}/τ_0 in a fixed area of size 12 mm×12 mm, with a=1 mm, $\omega_1 = \omega_2$=4a, τ_0=100 MPa, and k=1. The stress fields were very similar to the prediction results. For example, the antiplane stress τ_{zy} equaled zero on the crack surface. The singularity of the stress fields appeared in the crack tip area. Notably, the stress distribution was related to orthotropic parameters. It is well known that a shielding effect of multiple parallel cracks and an amplifying effect of multiple collinear cracks exist simultaneously in a DPRC problem. As can be seen from the contour plot of the stress τ_{zy}, the small orthotropic parameter improved the shielding effect of multiple parallel cracks, but the larger orthotropic parameter strengthened the amplifying effect of collinear cracks. For instance, compared with the results for C_{55}/C_{44}=10, the interference effect between collinear cracks was markedly weakened for C_{55}/C_{44}=0.5. Thus, a small orthotropic parameter can effect a decrease in stress concentration and further reduce the corresponding SIF. This is a good explanation of the variation of SIF with the orthotropic parameter shown in Fig. 3.

3.3 Crack tearing displacement

The displacement across the crack faces can be transformed into

$$w(x,0)=\begin{cases}\dfrac{\tau_0}{C_{44}}\dfrac{\pi}{m}\sum_{j=0}^{m}\left[\left(\sum_{n=0}^{\infty}\dfrac{1}{n\gamma k}\sin(n\gamma a s_j)\cos(n\gamma x)\right)\delta_j F(s_j)\right], y>0\\ \dfrac{\tau_0}{C_{44}}\dfrac{\pi}{m}\sum_{j=0}^{m}\left[\left(\sum_{n=0}^{\infty}\dfrac{-1}{n\gamma k}\sin(n\gamma a s_j)\cos(n\gamma x)\right)\delta_j F(s_j)\right], y<0\end{cases}. \tag{29}$$

Then, the CTD across the crack faces can be obtained by considering $\Delta w = w^{+} - w^{-}$.

In the following, the single crack problem for an infinite isotropic material is discussed and its corresponding CTD is calculated. For ease of discussion, the result of the single crack problem will be used as a reference value to normalize the CTD results presented for the DPRC problem.

For an infinite isotropic material containing a single central crack with length 2*a*, the following integral equation can be obtained by the integral equation method:

$$\frac{1}{2\pi}\int_{-a}^{a}\frac{1}{u-x}a_l(u)\,du=\frac{\tau_0}{C_{44}}. \tag{30}$$

This equation has the following analytical solution:

$$a_l(x)=\frac{2\tau_0}{C_{44}}\frac{x}{\sqrt{a^2-x^2}}, \tag{31}$$

and the corresponding CTD can be obtained:

$$w\left(x,0^{+}\right)-w\left(x,0^{-}\right)=\int_{x}^{a}a_l(u)\,du=\frac{2\tau_0}{C_{44}}\int_{x}^{a}\frac{u}{\sqrt{a^2-u^2}}du=\frac{2\tau_0\sqrt{a^2-x^2}}{C_{44}}. \tag{32}$$

Further, one can define the normalized CTD (NCTD) as the ratio of the CTD value for the DPC problem to the maximum displacement value of the CTD for the single crack problem:

$$w_0(x,y)=\frac{\Delta w(x,y)C_{44}}{2\tau_0 a}. \tag{33}$$

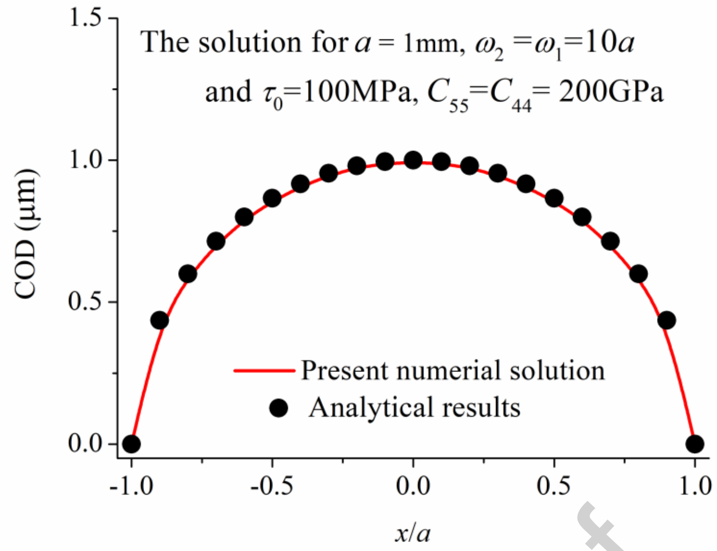
The solution for a = 1mm, $\omega_2=\omega_1=10a$
and τ_0=100MPa, $C_{55}=C_{44}$= 200GPa
Present numerial solution
Analytical results
COD (μm)
1.5
1.0
0.5
0.0
-1.0
-0.5
0.0
0.5
1.0
x/a

(a)

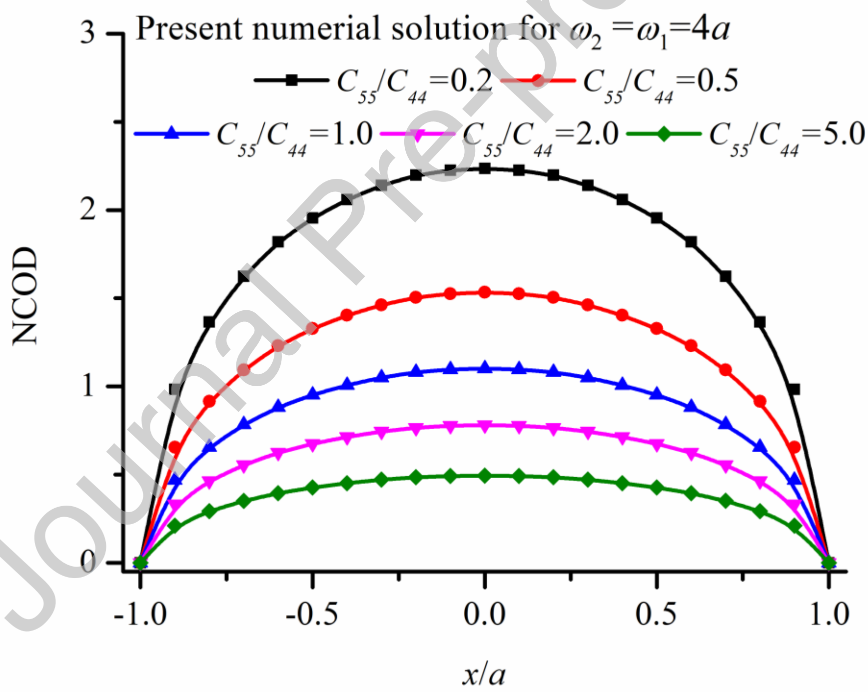
Present numerial solution for $\omega_2=\omega_1=4a$
C_{55}/C_{44}=0.2
C_{55}/C_{44}=0.5
C_{55}/C_{44}=1.0
C_{55}/C_{44}=2.0
C_{55}/C_{44}=5.0
NCOD
3
2
1
0
-1.0
-0.5
0.0
0.5
1.0
x/a

(b)

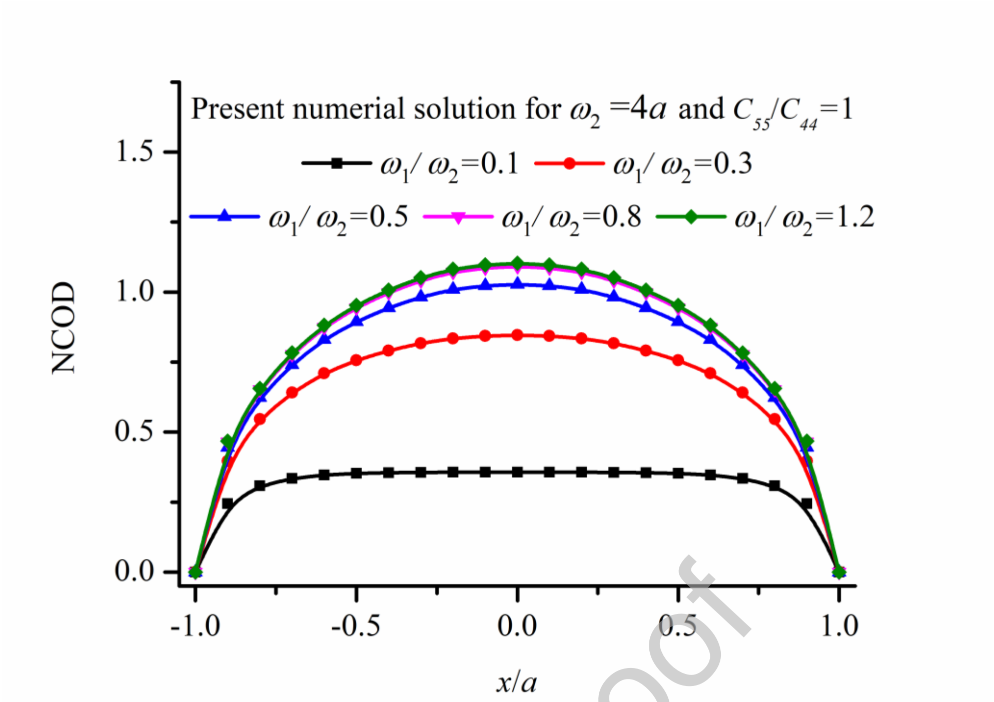

(c)

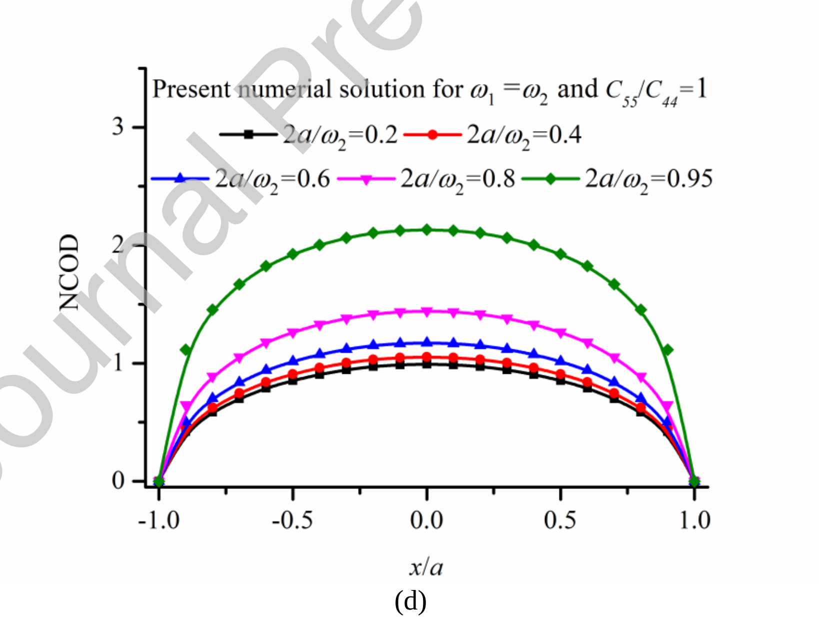

(d)

Fig. 5. Effects of periodic parameters and orthotropic parameter on CTD.

Here, the CTD results for the DPC problem obtained in the present work are compared with the analytical results for the single crack problem. In this paper, the parameters selected for solving the DPC problem satisfied $\omega_1 = \omega_2$=10a. As the doubly period parameter was much larger than the crack size, the interaction between the DPC was weak; thus, the DPC problem solved here can be considered to be equivalent to a single crack problem. As shown in Fig. 5(a), the calculation results were completely consistent with the analytical solution for the single crack problem, confirming that the proposed numerical method could solve the CTD across the crack surface with high accuracy. Further, Fig. 5(b–d) shows the influences of periodic parameters and orthotropic parameter ratio on NCTD. Increased crack size, increased crack longitudinal spacing, and decreased orthotropic parameter all led to increases in NCTD. The NCTD value showed a trend of increasing first and then gradually stabilizing with increasing vertical periodic parameter. When the vertical periodic parameter of the crack reached about twice the crack length, the NCTD no longer increased with further increases in the vertical periodic parameter. With decreasing crack size, the NCTD value exhibited a trend of decreasing first and then gradually stabilizing. When the crack size was less than one-fifth of the horizontal parameter of the crack, the NCTD no longer decreased with decreasing crack size.

3.4 Effective antiplane shear modulus

For the array of cracks under consideration, the effective antiplane shear modulus along the *x*-axis, $C_x = C_{55}$, remained unchanged. The effective antiplane shear modulus along the *y*-axis, C_y, could be obtained using average field theory [11]:

$$C_y = \bar{\tau}_{zy} / \bar{\gamma}_{zy} , \tag{34}$$

where the overline denotes the average of a corresponding physical quantity. From the far-field stress condition, it follows that [11]

$$\bar{\tau}_{zy} = \tau_0 . \tag{35}$$

Owing to the symmetry of the problem, the antiplane displacement *w* on the upper unit cell boundary and that on the non-cracked region collinear with the crack were constants; these values are respectively denoted by w_A, w_B. The average strain $\bar{\gamma}_{zy}$ can be obtained as follows:

$$\bar{\gamma}_{zy} = \frac{w_A - w_B}{\omega_1 / 2} = \frac{\tau_0}{C_{44}} - \frac{w_B}{\omega_1 / 2} = \frac{\omega_1 \tau_0 - 2 w_B C_{44}}{C_{44} \omega_1} . \tag{36}$$

Substitution of Eqs. (36) and (37) into Eq. (35) yields

$$C_y = \frac{\tau_0 C_{44} \omega_1}{\omega_1 \tau_0 - 2 w_B C_{44}} = \frac{C_{44} \omega_1}{\omega_1 - 2 C_{44} \bar{w}_B} , \tag{37}$$

where $\bar{w}_B = w_B / \tau_0$ represents the strain generated by the unit load, and $\bar{w}_B$ is independent of applied loading as the linear elasticity assumption is satisfied.

Further, the dimensionless effective antiplane shear modulus along the *y*-axis can be defined as

$$C_0 = \frac{C_y}{C_{44}} = \frac{\omega_1}{\omega_1 - 2\bar{w}_B C_{44}}. \tag{38}$$

From Eq. (38), it is clear that the effective antiplane shear modulus is independent of applied loading for the linearly elastic stage.

Table 3 presents a comparison of the numerical results for the effective antiplane shear modulus with the previous analytical solutions [11] and the numerical solution obtained using the boundary element method [20]. This comparison shows that the numerical method has a very high efficiency in the general and elongated rectangular doubly periodic case and for orthotropic solids. The comparison of numerical solutions proves that the proposed method also has high precision.

The variation of the effective antiplane shear modulus C_0 is displayed in Fig. 6. As shown in Fig. 6(a), the finite element results [11] coincided with the numerical solution. Fig. 6(b) provides a comparison between the numerical results and the analytical solutions. For various configurations of doubly periodic parameters, the numerical results were in good agreement with the analytical solutions. Furthermore, the effective antiplane shear modulus C_0 increased with increasing vertical periodic parameter, because the number of cracks per unit area decreased as the vertical periodic parameter increased. The effective antiplane shear modulus C_0 also increased monotonously with increasing C_{55}/C_{44}, possibly owing to the increased overall stiffness of the material. In addition, when C_{55}/C_{44} and ω_2/ω_1 were fixed, the effective modulus decreased with increasing a/ω_1.

Table 3. Comparison of dimensionless effective antiplane shear modulus for the BEM results, analytical solutions, and proposed numerical solutions

$2a/\omega_2$	0.1	0.2	0.3	0.4	0.5	0.6	0.7	0.8	0.9
C_{55}/C_{44}=1, $\omega_1=\omega_2$									
Present solutions	0.99217	0.96905	0.93164	0.88133	0.81967	0.74776	0.66613	0.57292	0.45909
Analytical solutions [11]	0.9922	0.9691	0.9316	0.8813	0.8196	0.7478	0.6661	0.5728	0.4590
BEM solutions [20]	0.9922	0.9691	0.9317	0.8814	0.8198	0.7480	0.6664	0.5731	0.4593
C_{55}/C_{44}=10, $\omega_1=\omega_2$									
Present solutions	0.99751	0.98999	0.97729	0.95908	0.93479	0.90335	0.86284	0.80884	0.72818
Analytical solutions [11]	0.9975	0.9900	0.9773	0.9591	0.9348	0.9034	0.8628	0.8088	0.7281
BEM solutions [20]	0.9975	0.9900	0.9773	0.9591	0.9348	0.9035	0.8630	0.8090	0.7284
C_{55}/C_{44}=0.1, $\omega_1=\omega_2$									
Present solutions	0.97610	0.91365	0.82955	0.73578	0.63817	0.53898	0.43928	0.33907	0.23595
Analytical solutions [11]	0.9761	0.9137	0.8296	0.7358	0.6381	0.5390	0.4393	0.3390	0.2359
BEM solutions [20]	0.9761	0.9137	0.8297	0.7359	0.6383	0.5392	0.4395	0.3392	0.2361

C_{55}/C_{44}=1, ω_1=0.05ω_2									
Present solutions	0.92192	0.82200	0.72202	0.62205	0.52207	0.42209	0.32209	0.22212	0.12214
Analytical solutions [11]	0.9220	0.8221	0.7221	0.6221	0.5221	0.4221	0.3221	0.2221	0.1221
BEM solutions [20]	0.9221	0.8222	0.7222	0.6222	0.5222	0.4221	0.3222	0.2222	0.1222
Maximum error									
Present solutions	<0.0001	<0.0001	<0.0001	<0.0001	<0.0001	<0.0001	<0.0001	<0.0001	<0.0001
BEM solutions	0.0001	0.0001	0.0001	0.0001	0.0002	0.0002	0.0002	0.0002	0.0003

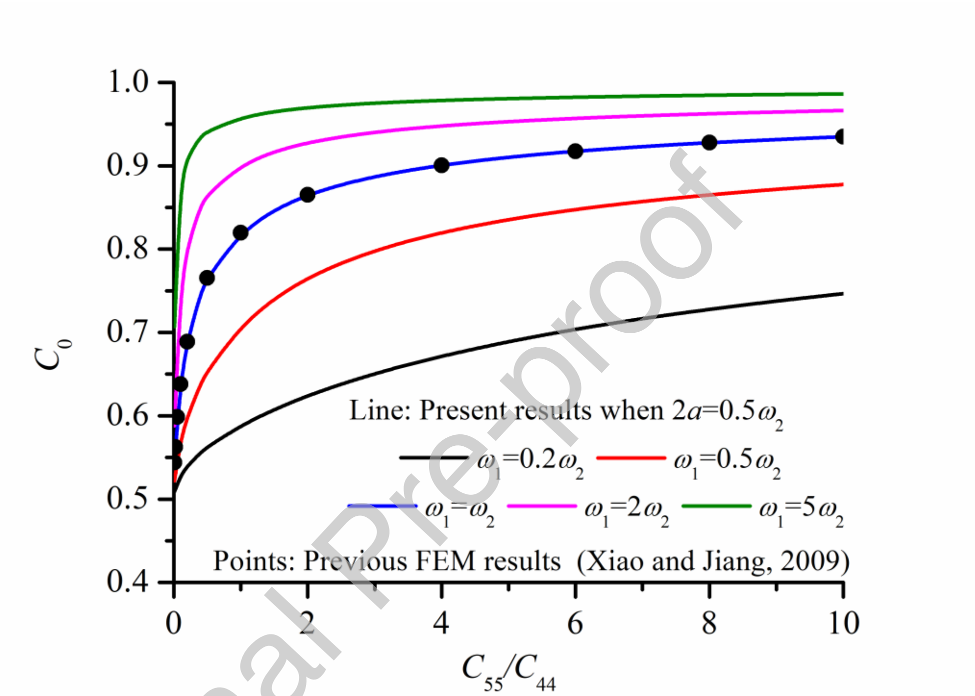

(a)

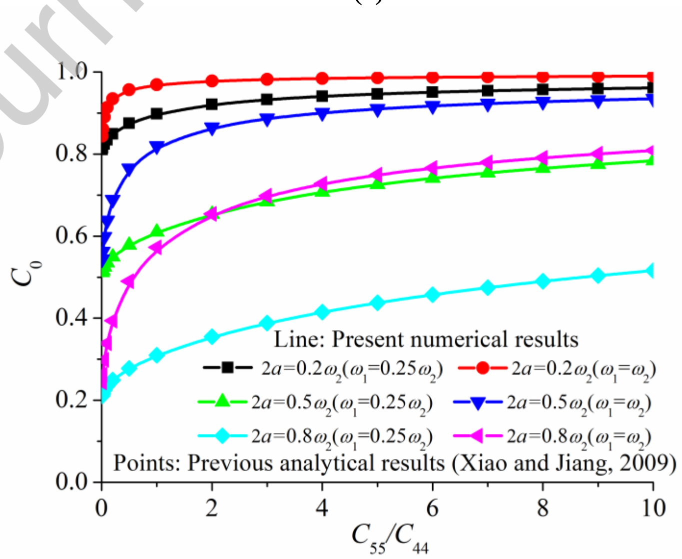

(b)

Fig. 6. Comparison of the effective modulus C_0 from finite element results and from the present solution.

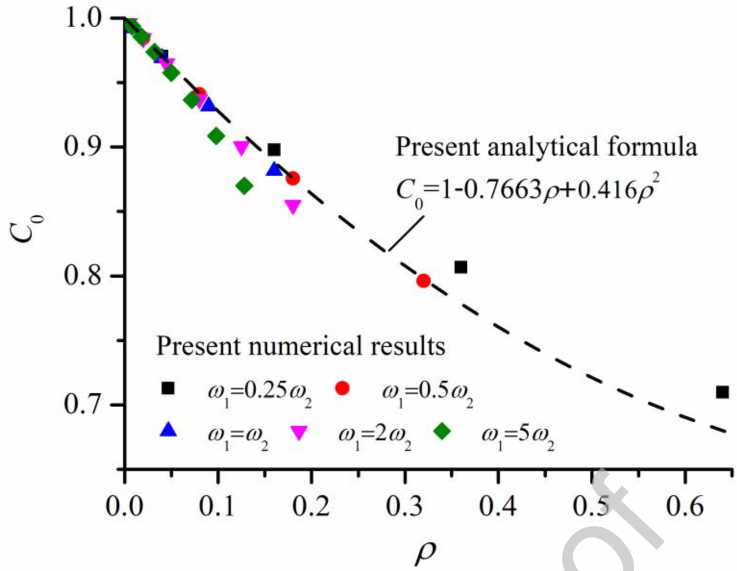

(a)

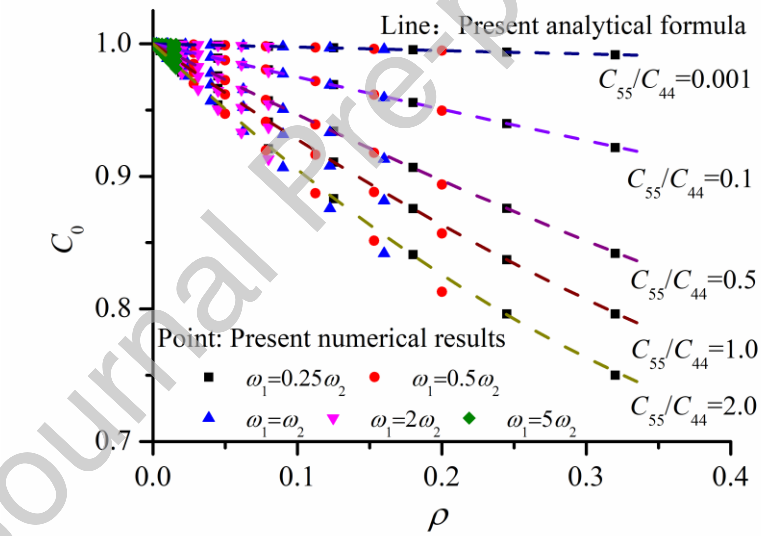

(b)

Fig. 7. Polynomial series formulae for the effective modulus C_0.

It is possible to obtain the values of SIF, OTD, and effective modulus C_0 for various combinations of crack half-length a, doubly periodic parameter ω_1 and ω_2, and orthotropic parameter C_{55}/C_{44}. However, in some cases, a singular integral equation must be solved numerically to obtain the required values. Even when using the analytic solution based on elliptical function theory and the conformal mapping technique [10,11], a complex numerical calculation of Jacobi elliptic function cannot be avoided. For convenience, we aimed to construct a polynomial series formula for the effective shear modulus C_0. Figure 7(a) gives an estimate of the effective shear modulus C_0 of an isotropic material:

$$C_0 = 1 - 0.7663\rho + 0.416\rho^2 , \quad (39)$$

where $\rho = 4a^2/(\omega_1\omega_2)$ represents the density of cracks.

For orthotropic materials, the estimated expression of the effective shear modulus C_0 becomes more complicated. In the case satisfying $C_{55}/C_{44}>0.5$, $\omega_1/\omega_2>0.5$, and $2a/\omega_2<0.5$, we obtained the following polynomial analytical formulae with higher precision by fitting

$$C_0 = F(\rho,\mu) = 1 - 0.02322\rho\left(1 + 122.5\mu - 243.6\mu^2 + 209.6\mu^3 - 56.5\mu^4\right) + 0.416\mu\rho^2 , \quad (40)$$

where $\rho = 4a^2/(\omega_1\omega_2), \mu = C_{44}/C_{55}$. Here, Eq. (39) is matched with Eq. (40) by setting $\mu = 1$.

Values of our polynomial analytical formulae are plotted in Fig. 7, with dashed lines showing close agreement with the numerical solution, under various parameter combinations shown as points.

3.5 Crack size studies

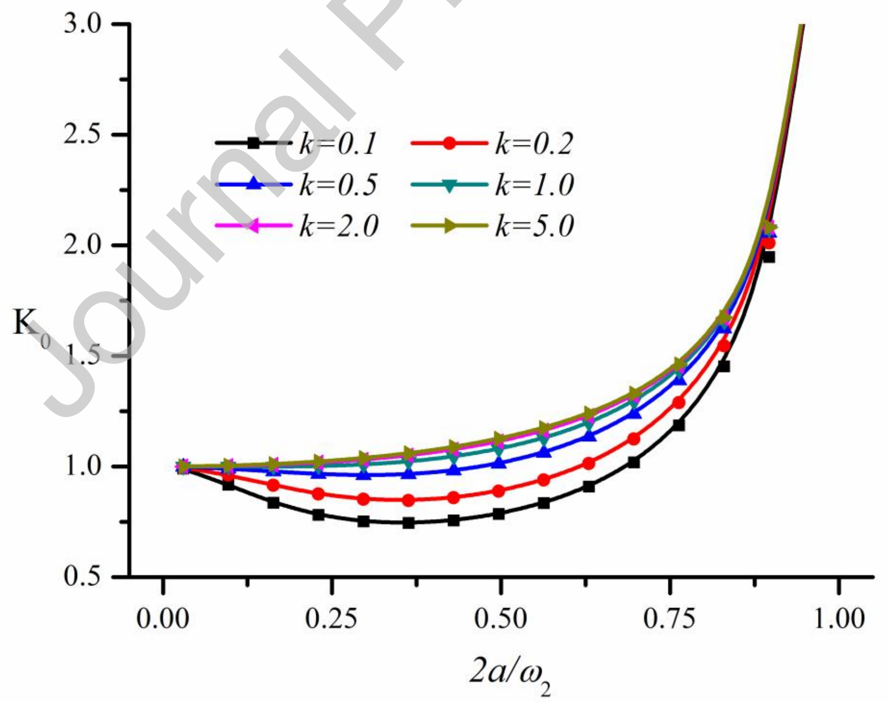

Fig. 8. Variation in SIFs versus crack size a for ω_1/ω_2=0.5.

The variation in SIF versus the crack size a is shown in Fig. 8, where ω_1 =3 mm and ω_2=6 mm. The SIF increased with increasing crack size when the crack size $2a$ was greater than $0.5\omega_2$.

In addition, as can be seen in Fig. 8, the SIF increased steeply as the crack size $2a$ approached the horizontal periodic parameter ω_2. Notably, the materials were mostly in a complete failure state as the crack size approached the half-length of the horizontal periodic parameter ω_2. Therefore, the SIF showed a rapid increase when the materials approached failure conditions.

4. Simple discussion of dynamic problem

By combining elliptical function theory and the conformal mapping technique, analytical solutions can be obtained for some special DPC problems [9–11]. However, this analytic method is based on a complex function method. For many complex DPC antiplane problems (e.g., composite materials, elastoplastic problems, and dynamic problems), the antiplane displacement field can no longer be expressed by the real parts of analytical functions; this will result in a failure to solve some complex DPC problems using the analytical method proposed in Refs [9–11]. It should be noted that the method proposed in this paper could be extended to various complex DPC problems, such as the elastoplastic DPC problem [22] and the DPC problem in periodic layered composites [23]. In addition, the presence of an infinite number of cracks leads to some difficulties in obtaining high-precision and fast solutions using the finite element method. Here, we propose an efficient and fast numerical method based on the singular integral equation method. In particular, when the number of numerical nodes is equal to 20, the absolute error of the calculation results is less than one in ten-thousand. In addition, the computational time required for one case is about 0.0084 sec. The numerical program was run on a PC with an Intel i7-7770 @ 3.60 GHz 64-bit processor, using MATLAB R2014a for Windows 10.

In the work described above, the static problem of orthotropic solids weakened by DPRC under a longitudinal shear load was solved. In this section, the dynamic behavior of orthotropic solids weakened by DPRC is investigated. In dynamic problems, the distribution of cracks and material parameters are consistent with those of static problems, but it is assumed that the propagation direction of the harmonic elastic antiplane shear stress wave is vertical to the cracks. Let ω be the frequency of the incident wave, and let $w(x,y,t)$ denote the mechanical displacement, and $\tau_{zx}(x,y,t)$ and $\tau_{zy}(x,y,t)$ the antiplane shear stress field. For this harmonic problem, all the field quantities of $w(x,y,t)$, $\tau_{zx}(x,y,t)$, and $\tau_{zy}(x,y,t)$ can be assumed to be in the following form [31]:

$$\left\{w(x,y,t),\tau_{zx}(x,y,t),\tau_{zy}(x,y,t)\right\}=\left\{w(x,y),\tau_{zx}(x,y),\tau_{zy}(x,y)\right\}e^{-i\omega t} \tag{41}$$

In what follows, the time dependence of $e^{-i\omega t}$ will be omitted. The DPRC boundary value problem for the harmonic antiplane shear waves can be simplified by considering the displacement only.

The stress should satisfy the following equilibrium equations:

$$\frac{\partial\tau_{zx}}{\partial x}+\frac{\partial\tau_{zy}}{\partial y}=\rho\frac{\partial^2 w}{\partial t^2}\,. \tag{42}$$

Substituting Eq. (1) into Eq. (42) yields the following governing equation:

$$k^2\frac{\partial^2 w}{\partial x^2}+\frac{\partial^2 w}{\partial y^2}+l^2 w=0\,, \tag{43}$$

where $l=\omega/c.$ $c=\sqrt{C_{44}/\rho}$ is the shear wave velocity and ρ denotes the mass density.

By applying the separation of variables method, the displacement w and stresses τ_{zx} and τ_{zy} can be written as:

$$w(x,y)=\begin{cases}\sum\limits_{n=0}^{\infty}[A(n)e^{\sqrt{n^2\gamma^2k^2-l^2}\,y}+B(n)e^{-\sqrt{n^2\gamma^2k^2-l^2}\,y}]\cos(n\gamma x), y>0\\ \sum\limits_{n=0}^{\infty}[C(n)e^{\sqrt{n^2\gamma^2k^2-l^2}\,y}+D(n)e^{-\sqrt{n^2\gamma^2k^2-l^2}\,y}]\cos(n\gamma x), y<0\end{cases} \tag{44}$$

$$\tau_{zx}(x,y)=\begin{cases}-\sum\limits_{n=0}^{\infty}C_{55}n\gamma\left[A(n)e^{\sqrt{n^2\gamma^2k^2-l^2}\,y}+B(n)e^{-\sqrt{n^2\gamma^2k^2-l^2}\,y}\right]\sin(n\gamma x), y>0\\ -\sum\limits_{n=0}^{\infty}C_{55}n\gamma\left[C(n)e^{\sqrt{n^2\gamma^2k^2-l^2}\,y}+D(n)e^{-\sqrt{n^2\gamma^2k^2-l^2}\,y}\right]\sin(n\gamma x), y<0\end{cases} \tag{45}$$

$$\tau_{zy}(x,y)=\begin{cases}\sum\limits_{n=0}^{\infty}C_{44}\sqrt{n^2\gamma^2k^2-l^2}\left[A(n)e^{\sqrt{n^2\gamma^2k^2-l^2}\,y}-B(n)e^{-\sqrt{n^2\gamma^2k^2-l^2}\,y}\right]\cos(n\gamma x), y>0\\ \sum\limits_{n=0}^{\infty}C_{44}\sqrt{n^2\gamma^2k^2-l^2}\left[C(n)e^{\sqrt{n^2\gamma^2k^2-l^2}\,y}-D(n)e^{-\sqrt{n^2\gamma^2k^2-l^2}\,y}\right]\cos(n\gamma x), y<0\,.\end{cases} \tag{46}$$

Following the process used to solve the static problem, a new Hilbert kernel singular integral equation of the first kind can be obtained for the dynamic DPRC problem:

$$\int_{-1}^{1}\left[\frac{1}{2}\cot\frac{\gamma a\left(s-r\right)}{2}-\sum_{n=0}^{\infty}\frac{2\sin(n\gamma as)\cos(n\gamma ar)}{1-e^{\sqrt{n^2\gamma^2k^2-l^2}\,\omega_1}}\right]a_l^{*}(s)ds=\frac{\tau_0\omega_2 n\gamma}{aC_{44}\sqrt{n^2\gamma^2k^2-l^2}}\,. \tag{47}$$

Again referring to the process used to solve the static problem, we can numerically solve the singular integral equation and analyze the SIFs, CTDs, and effective shear modulus of an infinite orthotropic solid with DPRC subjected to harmonic longitudinal shear stress waves.

Figure 9 shows a contour plot of the amplitude of the dimensionless stress τ_{zy}/τ_0 in a fixed area of size 8 mm×8 mm, with a=1 mm, $\omega_1 = \omega_2$=4a, τ_0=100 MPa, and k=1. As shown in Fig. 9(a) and (c), the peak and valley of the stress field were evenly distributed on the rectangular lattice array in the absence of defects. In the figure, the red zone represents stress values greater than 0 and the blue zone represents those less than 0; the red and blue zones have the same shape and size and are alternately arranged. When the circular frequency of the incident waves was la=2, compared with the results shown in Fig. 9(a), Fig. 9(b) revealed that the presence of cracks caused a change in the stress pattern at the left and right ends of the crack. This caused a rearrangement of the stress in the upper and lower crack and in the crack tip region; the area of the stress patch was reduced and it assumed an elongated elliptical shape. When the circular frequency of the incident waves was la=4, a comparison of the results shown in Fig. 9(c) and (d) revealed a more complex rearrangement of the stress map, in which the blue zone on the upper and lower surfaces of the crack split and grew in the y direction, overlapping the nearby red zone. The appearance of DPRC caused changes in the stress in the vicinity of the cracks, leading to changes in the overall contour plot.

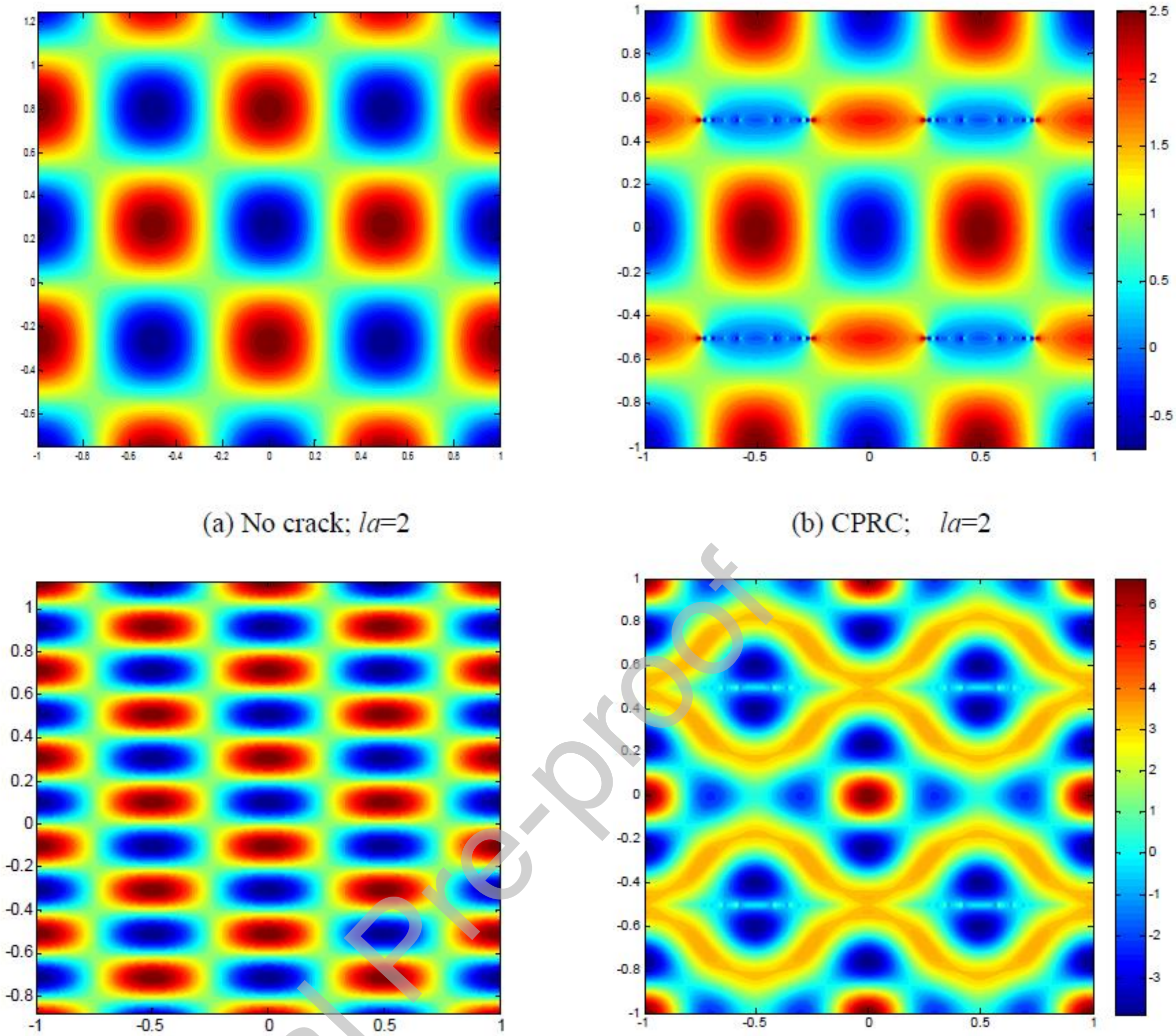

(a) No crack; *la*=2 (b) CPRC; *la*=2

(c) No crack; *la*=4 (d) CPRC; *la*=4

Fig. 9. Contour plot of dimensionless stresses τ_{zy}/τ_0 with incident waves of different frequencies.

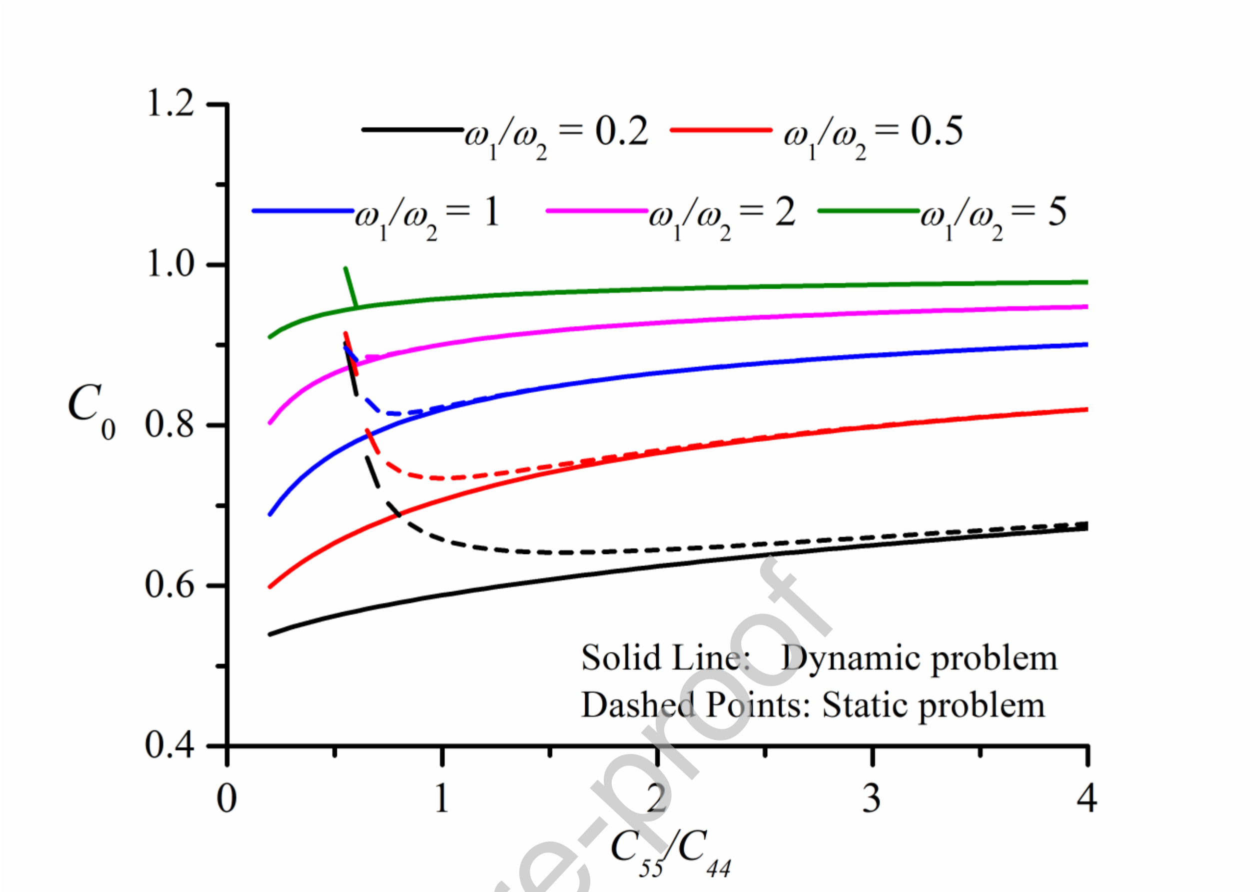

(a)

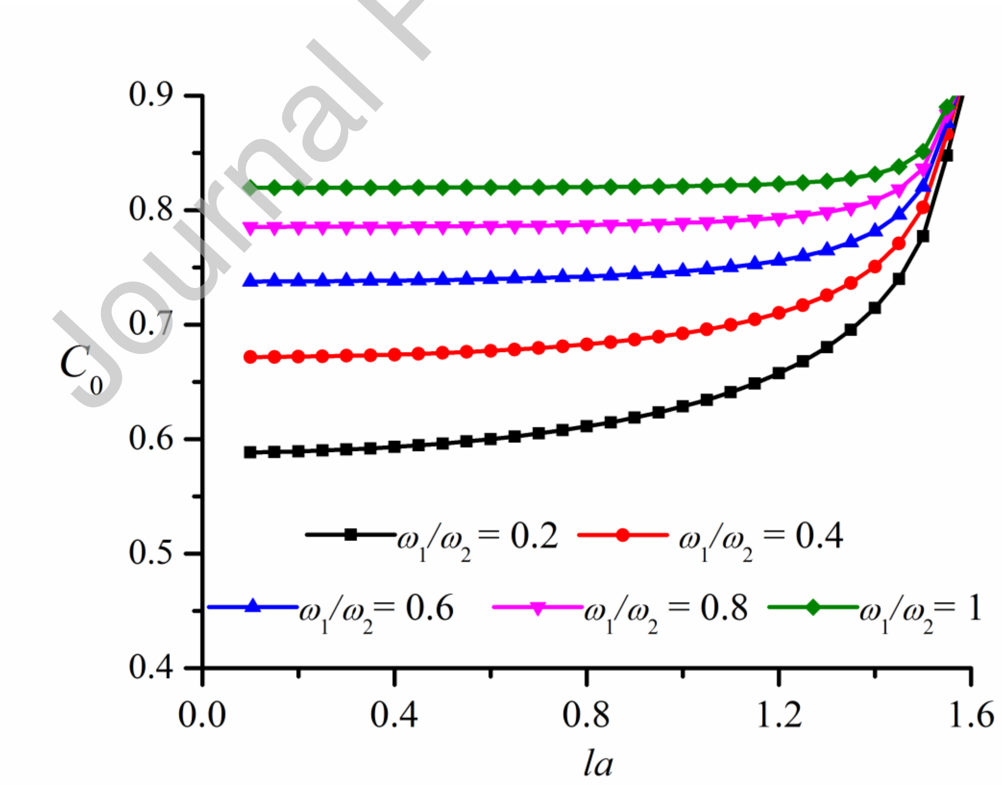

(b)

Fig. 10. Dynamic effects on the effective modulus C_0.

Figure 10 presents further analysis of the dynamic effects on the equivalent modulus. As shown in Fig. 10(a), the harmonic longitudinal shear stress waves led to an enhancement of the equivalent modulus. The effect decreased as the modulus increased and gradually approached the results obtained in the static situation. As the circular frequency of the incident waves *la* increased, as shown in Fig. 10(b), the dynamic effect gradually increased and the equivalent modulus increased.

5. Conclusions

The natural and highly accurate solution presented here enables study of the DCRP problem for orthotropic solids using a continuously distributed dislocation model. The advantage of the proposed method is that it can achieve high-precision numerical solutions for various physical quantities that are related to DPRC problems. Obtaining a high-precision numerical solution in this way makes full use of the symmetry of the unit cell and avoids errors caused by the summation of doubly infinite series. This paper summarizes and compares the existing analytical and numerical results for this problem, thereby confirming the effectiveness of the proposed numerical method for high-precision calculations of SIF, CTD, and effective shear modulus. In particular, polynomial analytical formulae for the effective shear modulus in a certain range are presented to facilitate the use of the results. The preliminary study of the dynamic problem performed here demonstrates the potential of this approach. Future work is expected to include a detailed study of solids containing doubly periodic strip-like cracks subjected to harmonic longitudinal shear stress waves.

Acknowledgments

Funding: This work was supported by the Fund of Natural Science Foundation of China [No. 11802225] and the Natural Science Basic Research Plan in the Shaanxi Province of China [Program No. 2019JQ-261].

The author also thanks the anonymous reviewers for careful reading of the manuscript and for their recommendations.

References

1. V.V. Panasyuk, M.P. Savruk, I.F. Soltys, Doubly periodic problem of thermal elasticity for a body with thermally isolated cracks. Soviet Materials Science, 11(1) (1976) 22–27.
2. M. Isida, H. Igawa, Doubly-periodic array and zig-zag array of cracks in solids under uniaxial tension, Int. J. Fracture 53(3) (1992) 249–260.
3. B.L. Karihaloo, Fracture characteristics of solids containing doubly-periodic arrays of cracks, Proc. R. Soc. Lond. A 360(1702) (1978) 373–387.
4. R. Sankar, A.J. Lesser, Generic overlapping cracks in polymers: modeling of interaction, Int. J. Fracture 142(3–4) (2006) 277–287.
5. X. Li, Complete plane strain problem of a nonhomogeneous elastic body with a doubly- periodic set of cracks, ZAMM 81(6) (2001) 377–391.
6. X. Li, The effect of a homogeneous cylindrical inlay on cracks in the doubly-periodic complete plane strain problem, Int. J. Fracture 109(4) (2001) 403–411.
7. S.S. Chang, The general solutions of the doubly periodic cracks, Eng. Fracture Mech. 18(4) (1983) 887–893.
8. Z.B. Kuang, The doubly-periodic rectangular array of cracks in problems of mode III, Acta Mech. Solida Sin. 2 (1985) 207–219.
9. T.H. Hao, An antiplane problem of double period non-uniform crisscross distribution crack field, Int. J. Fracture 30(3) (1986) 223–227.
10. Z.H. Tong, C.P. Jiang, S.H. Lo, Y.K. Cheung, A closed form solution to the antiplane problem of doubly periodic cracks of unequal size in piezoelectric materials, Mech. Mater. 38(4) (2006) 269–286.
11. J.H. Xiao, C.P. Jiang, Exact solution for orthotropic materials weakened by doubly periodic cracks of unequal size under antiplane shear, Acta Mech. Solida Sin. 22(1) (2009) 53–63.
12. J.H. Xiao, Y.L. Xu, C.P. Jiang, Exact solution to the antiplane problem of doubly periodic conducting rigid line inclusions of unequal size in piezoelectric materials, ZAMM 91(5) (2011) 413–424.
13. J.H. Xiao, Y.L. Xu, F.C. Zhang, Interaction between periodic cracks and periodic rigid-line inclusions in piezoelectric materials, Acta Mech. 224(4) (2013), 777–787.
14. B.L. Karihaloo, J. Wang, Grzybowski M, Doubly periodic arrays of bridged cracks and short fibre-reinforced cementitious composites, J. Mech. Phys. Solid. 44(10) (1996) 1565–1586.
15. B.L. Karihaloo, J. Wang, On the solution of doubly periodic array of cracks. Mech. Mater. 26(4) (1997) 209–212.
16. B.L. Karihaloo, J. Wang, Micromechanical modelling of strain hardening and tension softening in cementitious composites, Comput. Mech. 19(6) (1997) 453–462.
17. Pak YE, Goloubeva E, Electroelastic properties of cracked piezoelectric materials under longitudinal shear, Mech. Mater. 24(4) (1996) 287–303.
18. P. Malits, Doubly periodic array of thin rigid inclusions in an elastic solid, Quart. J. Mech. Appl. Math. 63(2) (2010) 115–144.
19. P. Yan P, C.P. Jiang, An eigenfunction expansion-variational method based on a unit cell in analysis of a generally doubly periodic array of cracks, Acta Mech. 210(1–2) (2010) 117–134.
20. I. Pasternak, Doubly periodic arrays of cracks and thin inhomogeneities in an infinite magnetoelectroelastic medium, Eng. Anal. Bound. Elem. 36(5) (2012) 799–811.
21. T.D. Williams, W.J. Parnell, Effective antiplane elastic properties of an orthotropic solid weakened by a periodic distribution of cracks, Quart. J. Mech. Appl. Math. 67(2) (2014) 311–342.
22. P.P. Shi, On the plastic zone size of solids containing doubly periodic rectangular-shaped arrays of cracks under longitudinal shear, Mech. Res. Commun. 67 (2015) 39–46.
23. P.P. Shi Interaction between the doubly periodic interfacial cracks in a layered periodic composite: simulation by the method of singular integral equation, Theor. Appl. Fracture Mech. 78 (2015) 25–39.
24. J.D. Achenbach, C.H. Zhang, Reflection and transmission of ultrasound by a region of damaged material, J. Nondestruct. Eval. 9 (1990) 71–79
25. H. Lekesiz, N. Katsube, S.I. Rokhlin, R.R. Seghi, Effective spring stiffness for a planar periodic array of collinear cracks at an interface between two dissimilar isotropic materials. Mech. Mater. Int. J. 43(2) (2011) 87–98.
26. M.V. Golub, O.V. Doroshenko, A. Boström, Effective spring boundary conditions for a damaged interface between dissimilar media in three-dimensional case. Int. J. Solid. Struct. 81 (2016) 141–150.
27. V.V. Mykhas'kiv, I.Y. Zhbadynskyi, C. Zhang, On propagation of time-harmonic elastic waves through a double-periodic array of penny-shaped cracks. Eur. J. Mech. A-Solid 73 (2019) 306–317.

28. M.A. Sumbatyan, M.Y. Remizov, On 3D theory of acoustic metamaterials with a triple-periodic system of interior obstacles. Continuum Mech. Therm. 31 (2019) 1–14.
29. L. Federici, A. Piva, E. Viola, Crack edge displacement and elastic constant determination for an orthotropic material, Theor. Appl. Fracture Mech. 31(3) (1999) 173–187.
30. F. Erdogan, G.D. Gupta, Bonded wedges with an interface crack under anti-plane shear loading, Int. J. Fracture 11(4) (1975) 583–593.
31. J. Liang, Scattering of harmonic anti-plane shear stress waves by a crack in functionally graded piezoelectric/piezomagnetic materials, Acta Mech. Solida Sin. 20(1) (2007) 75–86.